Estimate of Orbiter Static Aeroelasticity Properties via FLEXSTAB

Ralph K. Cavin III* and J. N. Holyoak†
Texas A&M University, College Station, Texas

The theory underlying the use of rigid-model experimental data in FLEXSTAB aeroelasticity calculations is summarized. A description is given of the aerodynamic and structural models used in the calculation of Space Shuttle Orbiter aeroelasticity properties during the re-entry phase. The authors' experience with the use of pressure, nonlinear force and moment, and area-ratio correction methods in the Orbiter application is described and typical program output data are included. The inability of the program to correctly estimate differential control surface pressures and to accept external corrections for these terms is shown to be a major limitation in the Orbiter application.

I. Introduction

In the past decade, aeroelastic analysis methods have rapidly evolved from classical procedures using beamlike structural models and approximate aerodynamic models to more complex methods based upon finite-element structural and aerodynamic theories. The computer program FLEXSTAB, which was developed for NASA Ames by the Boeing Airplane Company, is representative of the current state-of-the-art in aeroelastic analysis methods.[1] FLEXSTAB uses the Woodward Aerodynamic approach in which the body is represented by a grid of constant pressure panels that have appropriate singularities associated with them to account for surface flow conditions, thickness effects, wing-body interference, etc. The program has the capability to generate a structural influence coefficient matrix based upon EI and GJ (beam bending and torsional stiffness) input data if a beamlike structural model is adequate, or it can accept a limited class of externally generated finite-element models as input data. Several provisions have been made in the program to utilize experimental data such as rigid force and moment data, pressure data, downwash data, etc. Program output includes vehicle deformation, effect of aeroelasticity on trim parameters, on differential pressures, increments in the static stability derivatives due to elasticity, etc. FLEXSTAB has successfully been applied to configurations such as the YF-12, B-52, and Boeing 707.[2]

This paper describes results that have been obtained to date from the application of FLEXSTAB to the problem of estimating Orbiter re-entry aeroelasticity properties. Since the geometry of the Orbiter is characterized by relatively thick, low-aspect-ratio wings and a fuselage with broad cross section in relation to its length and having a large base area with no aft-section fuselage taper, it is clear that the Orbiter provides a severe test for the linear inviscid aerodynamic theory used in FLEXSTAB. Indeed, it was found that when geometrically accurate aerodynamics models were used in the development of aerodynamic influence coefficients, the theoretical rigid airplane estimates for C_{L_α} were quite close to measured data for the Orbiter; however serious errors were observed in estimates for C_{L_0}, C_{M_0}, C_{D_0}, and smaller errors were observed in some of the control surface stability derivatives. As a consequence, most of the data described in this paper are based on the utilization of two external correction mechanisms provided by the program; namely, external force and moment data and external pressure correction data. A brief overview of the manner in which each of the correction terms is entered into the aeroelasticity calculations is given in Sec. II. Section III contains a description of the aerodynamic panelling and the structural node locations and degrees of freedom that were used in the aeroelasticity analysis. The data obtained for both subsonic and supersonic flight conditions based upon the use of external correction for aerodynamic terms are presented in Sec. IV. Finally, the data obtained from use of an "effective area" weighting scheme is described in Sec. V.

II. Use of Experimental Aerodynamic Data in Aeroelasticity Calculations

Many modern aeroelasticity programs, like FLEXSTAB, generate aerodynamic influence matrices which relate the flow incidence at panel j to the differential pressure induced across panel i. It is tempting to attempt to perform corrections on the entries in the influence matrix, since aeroelasticity calculations would then be based upon a valid aerodynamic representation. Unfortunately, because of the highly coupled nature of aerodynamic matrices, and due to the complex model construction, instrumentation and testing program required for the generation of required data, direct correction of the aerodynamic influence coefficient matrix is usually not practical. Two types of experimental data were utilized to obtain the aeroelastic data described in this paper. In this section, a brief overview of the procedure used in FLEXSTAB to incorporate rigid experimental pressure data into aeroelastic calculations is first given, and then the methods for utilizing nonlinear, rigid force and moment data are described.

The distributed aerodynamic forces expressed in the Reference (Mean) Axis System are

$$\{f^A\}_I = [T_{fT}]\,[\{f_M\}_I + [Q_I]\,[A_{P\theta}]\,(\{\psi_C\} + \{\theta^*\} + \{\psi_M\})] \tag{1}$$

where

$[T_{fT}]$ = transforms force components in local body axis systems to the Reference Axis System

Received Dec. 12, 1977; revision received Jan. 19, 1978.

Index category: Aeroelasticity and Hydroelasticity.

*Professor of Electrical Engineering, Telecommunications and Control Systems Laboratory, Electrical Engineering Dept. Member AIAA.

†Research Associate, Telecommunications and Control Systems Laboratory, Electrical Engineering Dept.

$\{f_M\}_I$ = an abbreviated notation for forces due to thickness effects, speed variations, and leading-edge correction calculations

$[Q_I]$ = a matrix that is used to perform appropriate coordinate transformations and pressure-to-force conversions

$[A_{P\theta}]$ = an aerodynamic influence coefficient matrix relating flow incidence to differential pressures (the entries in $[A_{P\theta}]$ are determined from linear inviscid potential flow theory)

$\{\psi_C\}$ = represents component incidence due to body camber

$\{\theta^*\}$ = represents component incidence due to elastic rotation

$\{\psi_M\}$ = represents component incidence due to motion variables

$$\{\psi_M\} = \{\psi_{\delta_e}\}\delta_{e_I} + \{\psi_{\delta_a}\}\delta_{a_I} + \{\psi_{\delta_r}\}\delta_{r_I} + \{\psi_\alpha\}\alpha_I + \{\psi_\beta\}\beta_I + \{\psi_P\}\frac{2\hat{P}_I}{b} + \{\psi_Q\}\frac{2\hat{Q}_I}{c} + \{\psi_R\}\frac{2\hat{R}_I}{b} \quad (2)$$

Each of the vectors $\{\psi_{\delta_e}\}$, $\{\psi_{\delta_a}\}$, etc., is computed in FLEXSTAB based on the geometry definition provided to the program. It is convenient to write Eq. (1) in the following form:

$$\{f^A\}_I = [T_{fT}]\{f_T^A\}_I \quad (3)$$

where the definition of $\{f_T^A\}_I$ which represents aerodynamic segment forces in local body axis systems, is apparent from Eq. (1).

Now, the structural node points do not normally coincide with the points on the aerodynamic panel grid at which aerodynamic forces are assumed to act. Thus, a force transformation from the aerodynamic segment forces to structural node forces is performed, resulting in a structural influence matrix defined with respect to the aerodynamic grid:

$$\{\theta^*\}_I = [\tilde{C}_{\theta T}]_I\{f_T^A\}_I \quad (4)$$

We can expand $\{f_T^A\}_I$ defined by Eq. (3) as

$$\{f_T^A\}_I = [Q_I][A_{P\theta}]\{\theta^*\} + \{f_T^A\}_I' \quad (5)$$

where $\{f_T^A\}_I'$ represents all force contributions *except* those due to elasticity. If Eq. (5) is used in Eq. (4) and $\{\theta^*\}$ is computed, the indicated result is

$$\{\theta^*\} = ([I] - [Q_I][A_{P\theta}][\tilde{C}_{\theta T}])^{-1}[\tilde{C}_{\theta T}]_I\{f_T^A\}_I' \quad (6)$$

The significance of Eq. (6) is that the elastic rotation vector is written in terms of motion and other variables so that Eq. (5) becomes

$$\{f_T^A\}_I = \left[[Q_I][A_{P\theta}]([I] - [Q_I][A_{P\theta}][\tilde{C}_{\theta T}]_I)^{-1} \times [\tilde{C}_{\theta T}]_I + [I]\right]\{f_T^A\}_I' \quad (7)$$

After some manipulation Eq. (7) can be written in the general form

$$\{f_T^A\}_I = ([I] + [\tilde{H}])\{f_T^A\}_I' \quad (8)$$

where it can be shown that, if a rigid airplane is assumed, $[\tilde{H}] \triangleq [0]$. Now the vector $\{f_T^A\}_I'$ can be written in expanded form using Eqs. (1, 3, and 5) as

$$\{f_T^A\}_I' = \{f_T^A\}_0' + \{f_T^A\}_\alpha'\alpha + \{f_T^A\}_\beta'\beta + \{f_T^A\}_{\delta_e}'\delta_e + \{f_T^A\}_{\delta_r}'\delta_r + \{f_T^A\}_{\delta_a}'\delta_a + \{f_T^A\}_{\hat{Q}}'\hat{Q} + \{f_T^A\}_{\hat{P}}'\hat{P} + \{f_T^A\}_{\hat{R}}'\hat{R} \quad (9)$$

The component $\{f_T^A\}_0'$ accounts for forces arising due to body shape that are independent of motion variables. Each of these force terms is based upon linear aerodynamic theory and is not dependent in any way upon vehicle elasticity. The local axis system normal forces are transformed into normal differential pressures via

$$\{\Delta C_P\} = [F_\Delta]\{f_T^A\}_I \quad (10)$$

so that an expansion similar to Eq. (9) can be written for rigid differential pressure coefficients, i.e.,

$$\{\Delta C_P\}^R = \{\Delta C_P\}_0^R + \{\Delta C_P\}_\alpha^R\alpha + \{\Delta C_P\}_\beta^R\beta + \ldots \quad (11)$$

Assume that experimental differential pressures are available for the rigid airplane and that these pressures can be adequately represented by

$$\{\Delta C_P\}_{\text{exp}}^R = \{\overline{\Delta C_P}\}_0^R + \{\overline{\Delta C_P}\}_\alpha^R\alpha + \{\overline{\Delta C_P}\}_\beta^R\beta \quad (12)$$

The FLEXSTAB program allows the user to directly enter pressure correction terms for $\{\Delta C_P\}_0^R$, $\{\Delta C_P\}_\alpha^R$, and $\{\Delta C_P\}_\beta^R$ in order to force these pressure coefficients in the expansion of Eq. (11) to be identical to $\{\overline{\Delta C_P}\}_0^R$, $\{\overline{\Delta C_P}\}_\alpha^R$, and $\{\overline{\Delta C_P}\}_\beta^R$, respectively. After these corrections have been made, the inverse transformation matrix, $[F_\Delta]^{-1}$, from Eq. (10) is used to compute $\{f_T^A\}_{I,C}'$, where the subscript C indicates "corrected." The total forces acting on the elastic airplane, written in the local coordinate systems, now becomes

$$\{f_T^A\}_{I,C} = [[I] + [\tilde{H}]]\{f_T^A\}_{I,C}' \quad (13)$$

These corrected aerodynamic forces are now transformed to the Reference Axis System, and total forces and moments are computed about the mass center of the vehicle. This linear combination of the forces written in Eq. (13) is written symbolically as

$$\{F_B^A\}_I = [T_B]([I] + [\tilde{H}])\{f_T^A\}_{I,C}' \quad (14)$$

Now it is clear that Eq. (14) has a general expansion of the form

$$\{F_B^A\}_I = \{\overline{F_B^A}\}_0^R + \{\overline{\Delta F_B^A}\}_0^E + \{\overline{F_B^A}\}_\alpha^R\alpha + \{\overline{\Delta F_B^A}\}_\alpha^E\alpha + \{\overline{F_B^A}\}_\beta^R\beta + \{\overline{\Delta F_B^A}\}_\beta^E\beta + \{F_B^A\}_{\delta_e}^R\delta_e + \{\Delta F_B^A\}_{\delta_e}^E\delta_e + \ldots \quad (15)$$

The bars written over the 0, α, and β total force coefficients indicate that these coefficients are affected by the pressure correction mechanism.

The force vector, $\{F_B^A\}_I$ is used in FLEXSTAB to represent the aerodynamic force contributions in trim calculations from the vehicle equations of motion. It sometimes happens that the linear expansion of Eq. (15) does not adequately represent

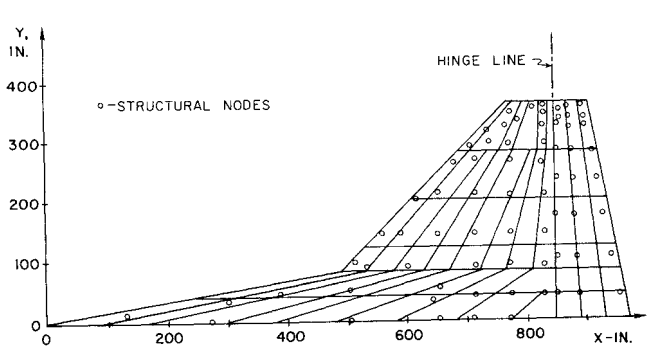

Fig. 1 Aerodynamic panels and structural node locations for Orbiter wing.

total aerodynamic forces and that improper trim solutions result. This problem is usually due to the fact that pressure corrections cannot be made for control surface differential pressures, although the problem can occur because of highly nonlinear vehicle aerodynamics. The FLEXSTAB user is provided the capability to represent the rigid force components in Eq. (15) by the use of tabular force and moment data. The linear terms, representing elastic force increments are retained. It is clear that when nonlinear force and moment data are provided to the program, a tacit *separability* assumption is made by the user with regard to elastic vehicle aerodynamic forces.

III. Shuttle Definition Data

A. Geometry

The user is required to define aircraft geometry in terms of a collection of thin and slender bodies. In the Orbiter problem, the wing and vertical tail were represented as thin bodies and the fuselage was represented as a slender body. Figure 1 depicts the wing planform and aerodynamic panelling scheme that were utilized. Similar data for the vertical tail are given in Fig. 2. In addition, thin body thickness and camber data were provided for both surfaces. The fuselage is approximated as a body of revolution having an associated interference body. A variety of interference-shell shapes were tried during the early phases of the study, however the configuration of Fig. 3 was finally chosen because it gave the best approximation to rigid aerodynamic forces and moments of all candidate shapes and because it provides a reasonable facsimile of actual aft-fuselage cross section.

B. Structural

In order to perform static aeroelastic analyses, the FLEXSTAB user is required to provide clamped structural, influence matrices and structural mass matrices as input data. If combined-maneuver studies are planned, then both symmetric and antisymmetric data are required. Although the program can generate the required structural matrices from a beamlike structural model, it was felt that such a representation is inadequate for the Orbiter. Therefore externally generated data were provided to the program.

The location of the wing structural nodes is shown as an overlay in Fig. 1. There are 71 wing nodes, each having z degrees of freedom only in the current structural model. The fuselage is represented with 12 structural nodes arranged along the centerline; each node having z degrees of freedom only in the current structural model. The fuselage is represented with 12 structural nodes arranged along the centerline; each node having x, y, and z degrees of freedom. Finally, the vertical tail structural node overlay is shown in Fig. 2, with each node retaining only y degrees of freedom. The resulting symmetric matrices are of dimension 95×95 and the antisymmetric matrices are dimensioned 132×132. (The difference is due to the fact that nodes located on the plane of symmetry and having y degrees of freedom appear only in the antisymmetric matrices.)

C. Aerodynamics

Both rigid wind tunnel force and moment data and differential pressure correction data were provided as input data to FLEXSTAB. Tabular force and moment data were used for both longitudinal and lateral degrees of freedom. The generation of pressure correction input data is somewhat more involved since pressure transducer locations do not normally coincide with the aerodynamic panel centroid locations used in FLEXSTAB. A bivariate cubic spline interpolation program was used to interpolate physical pressure measurements to the appropriate wing and vertical tail panel locations. The assumed linear form [Eq. (12)] did not accurately model the interpolated physical data, and thus the differential pressure coefficients were computed from physical data by least-squares curve-fit methods. It is clear that there can be no differential side force pressures when angle of attack is zero. Thus, on the vertical tail, the ΔC_{P_0} and ΔC_{P_α} terms were set to zero. It was observed that, for small angles of sideslip, wing differential pressures underwent negligible changes, and thus no ΔC_{P_β} corrections were generated for the wing aerodynamic nodes.

IV. Orbiter Aeroelasticity Data Using Corrections for both Total Forces and Distributed Pressures

Two flight conditions were selected from a nominal Orbiter re-entry trajectory for aeroelasticity analyses using FLEXSTAB with externally supplied aerodynamic data as described in Sec. III.C. Flight condition I corresponds to $M = 1.1$, $q_\infty = 162.6\ \text{lb}_\text{f}/\text{ft}^2$ and flight condition II is $M = 0.6$, $q_\infty = 126\ \text{lb}_\text{f}/\text{ft}^2$. The program was required to compute trim parameters for both of these flight conditions using both a rigid structural model and the elastic structural model described in Sec. II.B. Since linear pressure corrections were utilized for body shape, α, and β variables, and since corrections are not possible for the control surface variables, it was decided to compare computed FLEXSTAB differential pressures for the rigid vehicle with control surfaces deflected with differential pressures obtained from wind tunnel data at the same flight state. Figures 4 and 5 display experimental and computed differential pressures on the vertical tail at $M = 1.1$, $\alpha = 10$ deg, $\beta = 5$ deg, and $\delta_R = 10$ deg. Note that, near the leading edge of the vertical tail, there is good agreement

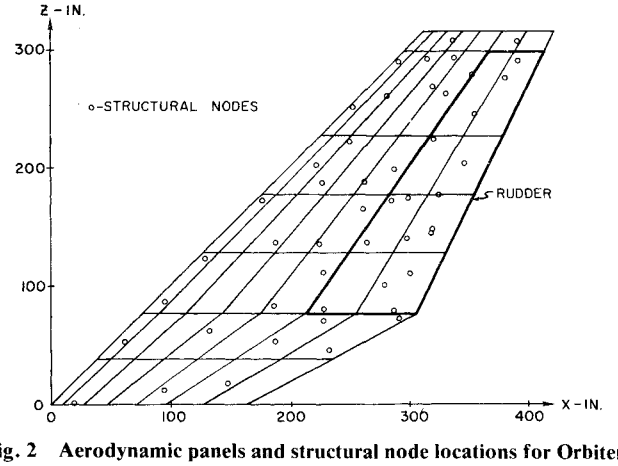

Fig. 2 Aerodynamic panels and structural node locations for Orbiter vertical tail.

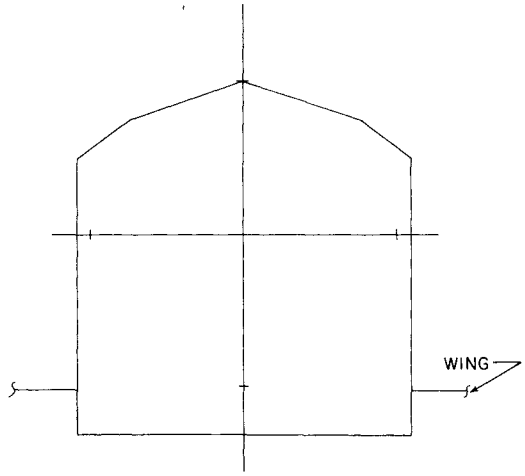

Fig. 3 Orbiter fuselage interference shell.

Table 1 Trim parameters for $\eta = 1g$, $Q = 0.01$ deg/s

Flight condition	Structure	α	θ	δ_e	β	δ_a	δ_r
I	rigid	6.31	−25.27	5.58	−0.135	−0.080	−0.118
I	elastic	6.30	−26.62	10.10	−0.136	0.124	−0.038
II	rigid	9.11	− 7.32	9.51	−0.103	0.033	−0.121
II	elastic	9.14	− 7.50	10.66	−0.144	0.131	0.448

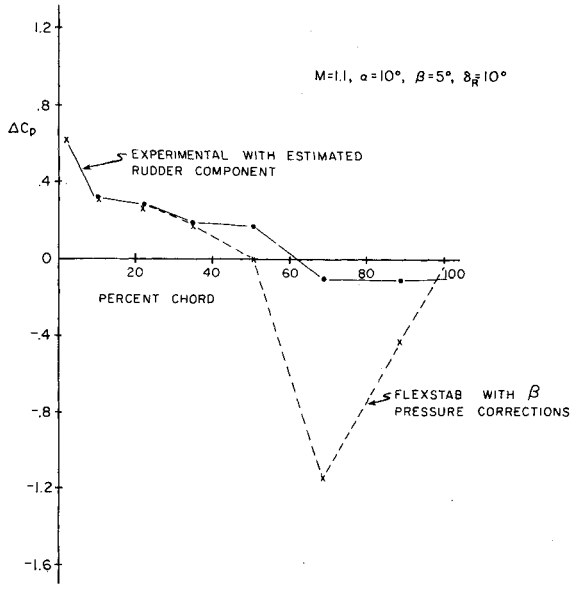

Fig. 4 Differential pressures vs percent local chord at 47% of vertical tail span.

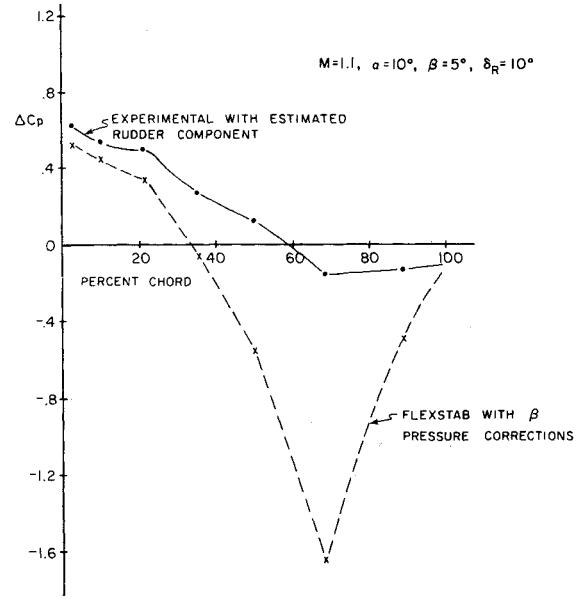

Fig. 5 Differential pressures vs percent local chord at 82.5% of vertical tail span.

between the two data sets. This is not unexpected since pressure corrections for α and β are included in the FLEXSTAB input data and since rudder deflections will have minimal effect on leading-edge differential pressures. However, from about 60% of local chord to the trailing edge, significant differential pressure errors are evident. The differential pressure estimates due to FLEXSTAB exceed actual differential pressure magnitudes by several hundred percent. A similar phenomenon was observed for the elevon differential pressures although errors were usually smaller. These errors are sufficiently large so that Orbiter aeroelasticity estimates using FLEXSTAB must be viewed as unreliable. It is possible that the very large rudder-related differential pressure errors are due in part to the blunt trailing edge of the rudder due to the speed brake.

Table 1 contains comparative trim data obtained for flight conditions I and II, at a 1-g normal load factor and with a perturbation yawing rate of 0.01 deg/s. The rigid and elastic increments in static stability derivatives for flight conditions I and II, computed at the trim points in Table 1, are given in Tables 2 and 3, respectively. Note that, in general, the trim solution components and the static stability derivatives that depend on α and β change very little between static and rigid cases. An exception is C_{n_β} which does show large elastic increments, especially at flight condition II. In contrast, the control surface variables generally exhibit large changes in both trim settings and static stability derivatives due to vehicle elasticity. These effects are in congruence with our earlier observation that Orbiter control surface differential pressures are incorrectly modelled by FLEXSTAB, and thus that control surface elastic increments are likely to be in error.

V. Area-Ratio Approach to Aeroelasticity Estimates

In view of the inaccuracies in FLEXSTAB estimates for control surface differential pressure components, it was decided to utilize the area-ratio option in which effective areas on which differential pressures are assumed to be acting are altered in order to achieve correct local forces. It is important to note that area ratios that are appropriate for a given set of flight parameters are generally not correct for any other set of parameters, even if a linear aerodynamic model is adequate. Consequently, the "Specified Trim" option in FLEXSTAB was utilized in order to delete trim calculations and to retain those flight conditions at which the area ratios were computed. The new effective areas are entered in the matrix $[F_\Delta]$ contained in Eq. (10) and utilized in subsequent elasticity calculations described in Sec. II. One of the principal concerns of this study was the estimation of the effects of aeroelasticity on lateral directional flight characteristics. The Orbiter vertical tail is relatively flexible, has a fairly high aspect ratio, and it was felt that there might be large lateral directional aeroelastic increments. Consequently, a specified trim run was conducted at flight condition I with $\alpha = 10$ deg, $\beta = 5$ deg, $\delta_R = 10$ deg, using externally supplied force and moment data, pressure corrections, and area-ratio data. The resulting lateral directional static stability derivatives are given in Table 4. If the data in Table 4 are compared to the data in Table 2, it is apparent that elastic increments in static stability derivatives using the area ratio terms are in the range of 10 to 20% of their rigid values, while the elastic increments computed without area ratios are generally in the range of 25 to 50% of rigid values. We believe, for reasons stated earlier, that the estimates of elasticity effects using the area-ratio method are the best that can be obtained for the Orbiter by use of the existing version of FLEXSTAB.

VI. Summary

An application of the aeroelasticity program FLEXSTAB, to the problem of estimating Space Shuttle Orbiter

Table 2 Estimated increments in static stability derivatives due to aeroelasticity at $\eta = 1g$, $Q = 0.01$ deg/s, flight condition I

Derivative	Rigid	Elastic increment	Total
C_{L_0}	−0.0582	0.0066	−0.0516
C_{D_0}	0.1829	−0.0009	0.18281
C_{m_0}	0.0835	−0.0050	0.0785
C_{L_α}	0.0579	−0.0006	0.0573[a]
C_{D_α}	0.0136	−0.0010	0.0126[a]
C_{m_α}	−0.0025	0.0006	−0.0019[a]
$C_{L_{\delta_e}}$	0.0109	−0.0055	0.0054[a]
$C_{D_{\delta_e}}$	0.0032	−0.0005	0.0027[a]
$C_{m_{\delta_e}}$	−0.0080	0.0037	−0.0043[a]
C_{Y_β}	−0.0196	0.0008	−0.0186[a]
C_{l_β}	−0.00225	0.00005	−0.0022[a]
C_{n_β}	0.00082	−0.00041	0.00041[a]
$C_{Y_{\delta_a}}$	0.00167	−0.00184	−0.00017[a]
$C_{l_{\delta_a}}$	−0.0027	0.0004	−0.0023[a]
$C_{n_{\delta_a}}$	−0.00047	0.00078	0.00031[a]
$C_{Y_{\delta_r}}$	0.00247	−0.00136	0.00111[a]
$C_{l_{\delta_r}}$	0.00077	−0.00036	0.00041[a]
$C_{n_{\delta_r}}$	−0.00130	0.00071	−0.00059[a]

[a] Units are deg.$^{-1}$

Table 3 Estimated increments in static stability derivatives due to aeroelasticity at $\eta = 1g$, $Q = 0.01$ deg/s, flight condition II

Derivative	Rigid	Elastic increment	Total
C_{L_0}	−0.0748	0.0029	−0.0719
C_{D_0}	0.0951	0.0001	0.0952
C_{m_0}	0.0511	−0.00189	0.04921
C_{L_α}	0.0529	−0.00052	0.05238[a]
C_{D_α}	0.01189	−0.00052	0.01137[a]
C_{m_α}	0.0023	0.00035	0.00265[a]
$C_{L_{\delta_e}}$	0.0184	−0.00199	0.01641[a]
$C_{D_{\delta_e}}$	0.00505	−0.00036	0.00469[a]
$C_{m_{\delta_e}}$	−0.00806	0.00075	−0.00731[a]
C_{Y_β}	−0.0187	0.0056	−0.0131[a]
C_{l_β}	−0.00210	0.00021	−0.00189[a]
C_{n_β}	0.0011	−0.0018	−0.0007[a]
$C_{Y_{\delta_a}}$	0.00387	−0.0020	0.00187[a]
$C_{l_{\delta_a}}$	−0.00398	0.00003	−0.00395[a]
$C_{n_{\delta_a}}$	−0.00088	0.00061	−0.00027[a]
$C_{Y_{\delta_r}}$	0.00245	−0.00330	−0.00085[a]
$C_{l_{\delta_r}}$	0.00072	−0.00017	0.00055[a]
$C_{n_{\delta_r}}$	−0.00122	0.00108	−0.00014[a]

[a] Units are deg^{-1}.

aeroelasticity properties has been described. Some of the underlying mathematical formulations that are used in the program to introduce external differential pressure corrections, wind tunnel force and moment data, and area-ratio data were examined. The geometry, structural, and aerodynamic models used to represent the Orbiter in FLEXSTAB were briefly described.

Table 4 Elastic increments in static stability derivatives based on the area-ratio load correction method: flight condition I, $\alpha = 10$ deg, $\beta = 5$ deg, $\delta_R = 10$ deg, and all flight variables are held to zero

Derivative	Rigid	Elastic increments	Total
C_{Y_β}	−0.01791	0.00067	−0.01724[a]
C_{l_β}	0.00024	−0.00005	0.00019[a]
C_{n_β}	0.00127	−0.00029	0.00098[a]
$C_{Y_{\delta_r}}$	0.00153	−0.00027	0.00126[a]
$C_{l_{\delta_r}}$	0.00024	−0.000045	0.000195[a]
$C_{n_{\delta_r}}$	−0.000751	0.00013	−0.00062[a]

[a] Units are deg^{-1}.

We observed that in the Orbiter application, FLEXSTAB gives very poor estimates for differential pressure components due to control surface deflections. This error is probably due to the inadequacy of the linear theory for airfoils whose trailing-edge cross section has a thickness which is large relative to the mean airfoil section thickness. The area-ratio mechanism can be used to achieve correct structural aerodynamic loads at a given flight condition; however, one must sacrifice the acquisition of data on aeroelasticity effects on trim. Unfortunately, there are no experimental aeroelasticity data available for the Orbiter, and it is not possible to substantiate our claims that the area-ratio data more accurately represents Orbiter aeroelasticity characteristics. It is apparent that many of the difficulties that were faced in the Orbiter application could have been minimized if FLEXSTAB had been provided the capability to accept control variable differential pressure corrections during program development. If the aircraft to be analyzed differs substantially from the collection of thin and slender bodies for which the linear aerodynamic theory is appropriate, we believe that the prospective user should validate control surface differential pressure estimates before proceeding with the aeroelastic analyses.

Acknowledgment

This work was supported by NASA Johnson Space Center under Contract NAS9-14478. Contract monitors were J. Young and E. Hillje, Engineering Analysis Division.

References

[1] Dusto, A.R., et al., "A Method for Predicting the Stability Characteristics of an Elastic Airplane; Volume I – FLEXSTAB Theoretical Description," Boeing Commercial Airplane Company, NASA CR 114712, Oct. 1974.

[2] Dusto, A.R., et al., "A Method for Predicting the Stability Characteristics of an Elastic Airplane; Volume IV – FLEXSTAB Demonstration Cases and Results," Boeing Commercial Airplane Company, NASA CR 114715, Oct. 1974.